AIP | Journal of Applied Physics

The induction of nanographitic phase on Fe coated diamond films for the enhancement in electron field emission properties

Kalpataru Panda, B. Sundaravel, B. K. Panigrahi, H.-C. Chen, P.-C. Huang, W.-C. Shih, S.-C. Lo, L.-J. Lin, C.-Y. Lee, and I.-N. Lin

Citation: Journal of Applied Physics **113**, 094305 (2013); doi: 10.1063/1.4792520
View online: http://dx.doi.org/10.1063/1.4792520
View Table of Contents: http://scitation.aip.org/content/aip/journal/jap/113/9?ver=pdfcov
Published by the AIP Publishing

The induction of nanographitic phase on Fe coated diamond films for the enhancement in electron field emission properties

Kalpataru Panda,[1,a)] B. Sundaravel,[1] B. K. Panigrahi,[1,b)] H.-C. Chen,[2,3] P.-C. Huang,[4] W.-C. Shih,[4] S.-C. Lo,[5] L.-J. Lin,[5] C.-Y. Lee,[2] and I.-N. Lin[3]
[1]*Materials Physics Division, Indira Gandhi Centre for Atomic Research, Kalpakkam 603 102, India*
[2]*Department of Materials Science and Engineering, National Tsing-Hua University, Hsinchu 300, Taiwan*
[3]*Department of Physics, Tamkang University, New Taipei 251, Taiwan*
[4]*Graduate Institute in Electro-Optical Engineering, Tatung University, Taipei 104, Taiwan*
[5]*Materials and Chemical Research Labs, ITRI, Hsinchu, Taiwan 310, Taiwan*

(Received 15 January 2013; accepted 4 February 2013; published online 7 March 2013)

A thin layer of iron coating and subsequent post-annealing (Fe-coating/post-annealing) is seen to significantly enhance the electron field emission (EFE) properties of ultrananocrystalline diamond (UNCD) films. The best EFE properties, with a turn on field (E_0) of 1.98 V/μm and current density (J_e) of 705 μA/cm^2 at 7.5 V/μm, are obtained for the films, which were Fe-coated/post-annealed at 900 °C in H_2 atmosphere. The mechanism behind the enhanced EFE properties of Fe coated/post-annealed UNCD films are explained by the microstructural analysis which shows formation of nanographitic phase surrounding the Fe (or Fe_3C) nanoparticles. The role of the nanographitic phase in improving the emission sites of Fe coated/post-annealed UNCD films is clearly revealed by the current imaging tunneling spectroscopy (CITS) images. The CITS images clearly show significant increase in emission sites in Fe-coated/post-annealed UNCD films than the as-deposited one. Enhanced emission sites are mostly seen around the boundaries of the Fe (or Fe_3C) nanoparticles which were formed due to the Fe-coating/post-annealing processes. Moreover, the Fe-coating/post-annealing processes enhance the EFE properties of UNCD films more than that on the microcrystalline diamond films. The authentic factor, resulting in such a phenomenon, is attributed to the unique granular structure of the UNCD films. The nano-sized and uniformly distributed grains of UNCD films, resulted in markedly smaller and densely populated Fe-clusters, which, in turn, induced more finer and higher populated nano-graphite clusters. © *2013 American Institute of Physics*. [http://dx.doi.org/10.1063/1.4792520]

I. INTRODUCTION

Microcrystalline diamond (MCD) films have many interesting physical and chemical properties[1–3] and are the focus of intensive research since the successful synthesis of diamond in the low pressure and low temperature chemical vapour deposition (CVD) process.[4] Negative electron affinity (NEA) properties of diamond films make it a suitable candidate for their application as electron field emitters.[5] Generally, a good electron field emitter requires sufficient supply of electrons from the back contact materials, effective transport of electrons through the material and efficient emission from the surface. The electron field emission (EFE) properties of large electronic band gap (5.5 eV) diamond films hinder the EFE process tremendously due to the lack of free electrons required for the emission processes. Recently, the newly developed diamond films with ultrananocrystalline diamond (UNCD) grain microstructure has drawn lot of attention[6–8] due to the fact that these materials possess physical and chemical properties, some of which are even superior to those of MCD films. The UNCD films contain large proportion of grain boundaries with considerable thickness.[7,8] The grain boundaries contain amorphous carbon phases, which are more conductive than at the grain boundaries of MCD films and thus resulted in markedly better EFE properties. However, the EFE properties of UNCD films are still not sufficiently good as compared with those of nano-carbon materials.[9–11] There are many approaches to modify the surface of diamond films to enhance their EFE properties. Among the various approaches, a thin layer of metallic coating (Au, Cr, Ni, Fe) improves the EFE properties of microcrystalline diamond films significantly.[12–16] Previous study shows improved EFE properties of MCD films by Fe coating and subsequent annealing processes.[14,16] It is expected that the same Fe-to-diamond interaction may also occur for the UNCD films. However, it is not clear whether the difference in granular structure between the MCD and UNCD films will impose different Fe-to-diamond interactions and resulted in different effects on the EFE properties of UNCD films.

In this context, we investigate in detail, the interaction of Fe-clusters with the UNCD films and its effect on the EFE properties. Transmission electron microscopy (TEM) is used to investigate the microstructural evolution of these films due to the Fe-coating and annealing processes, whereas scanning tunnelling spectroscopy (STS) in current imaging tunnelling spectroscopy (CITS) mode is used to directly examine the modification in emission sites in these UNCD films. The behavior of Fe-to-diamond interaction occurred on UNCD films is compared with those on MCD films and

[a)]Electronic mail: phy.kalpa@gmail.com.
[b)]Electronic mail: bkp@igcar.gov.in.

the possible mechanism that resulted in different enhancements in EFE of the two kind of diamond films is discussed on the basis of STS and TEM observations.

II. EXPERIMENTAL METHODS

Ultrananocrystalline diamond films were grown on p-type silicon substrates in a microwave plasma enhanced chemical vapour deposition (IPLAS-Cyrannus) system. The Si substrates were first thoroughly cleaned by the standard RCA cleaning procedure,[17] which includes the rinsing of the Si substrates in a water-diluted hydrogen peroxide/ammonium hydroxide and hydrogen peroxide/hydrochloric acid solution sequentially. Then the cleaned Si substrates were ultrasonicated in a solution containing nanodiamond and titanium powders (<32.5 nm) for 45 min to facilitate the nucleation of nanodiamond. The UNCD films were grown on the cleaned Si substrates in a $CH_4/H_2/Ar = 4/12/184$ sccm plasma excited by 1200 W (2.45 GHz) microwave power with 200 mbar pressure for 1 h. A thin layer of Fe (around 10 nm) was coated on the UNCD films by DC sputtering process for 1 min. The Fe coated UNCD films were annealed in H_2 atmosphere, with a flow rate of 100 sccm for 5 min with heating and cooling rate of around 15 °C/min. In the previous studies for MCD films,[14,16] it is known that the Fe-to-diamond interaction mainly occurred at 900 °C. Therefore, in the present study, we did the Fe coating and annealing processes for the UNCD films at the same high temperatures of 900 °C to study the effect of Fe-coating/post-annealing processes on the evolution of microstructure of diamond films on the reaction mechanism and its subsequent effect on EFE properties. The as-deposited and Fe-coated/post-annealed UNCD films at 900 °C are designated as $(UNCD)_0$ and $(Fe/UNCD)_{900}$, respectively.

A homebuilt tunable parallel plate capacitor setup was used to measure the EFE properties of these films. The EFE properties of the Fe coated/annealed films were analyzed using Fowler–Nordheim (F-N) model.[18] The surface morphology of the films was investigated by field emission scanning electron microscope (FESEM, CARL ZEISS, SUPRA 55). A high resolution diffractometer (GIXRD-STOE) at an angle of incidence of 0.2° was used to detect the new phase formed by the Fe coating and annealing processes. The Raman spectra were recorded using 514.5 nm line of an Ar-ion laser, by Renishaw micro-Raman spectrometer (Model-INVIA). Chemical bonding structures were investigated by XPS using SPECS made photoelectron spectrometer.

A commercial ultrahigh vacuum scanning tunneling microscopy (UHV-STM, 150 Aarhus, SPECS GmbH) was used to measure the local electronic properties of the films at a base pressure of 10^{-10} mbar. The STS spectra were obtained during scanning and the data presented here are reproducible over subsequent scans. CITS mode was used to correlate the STM image with its surface local density of states (DOS) distribution, which gives local conductivity mapping of the sample surface. CITS acquires a current versus voltage (I-V) curve, measured with the feedback loop off, in every point of the surface.[6] The detailed microstructure of the Fe coated/annealed UNCD films was examined using high resolution TEM (HRTEM, JEOL 2100). The elemental distributions of the species in these films were examined using the high angle annular dark field (HAADF) technique and the 3D-tomography in scanning TEM (STEM) mode. The 3D-tomography is the sequential replay of the HAADF images taken with the samples tilted step wisely (2°) using a software DIGITAL-MICROGRAPH (JEOL).[19]

III. RESULTS

A. General characteristics

The FESEM images of the $(UNCD)_0$ and $(Fe/UNCD)_{900}$ films are shown in Fig. 1, indicating that the surface morphology of the UNCD films was modified significantly due to the 900 °C Fe coating/annealing processes. Notably, no change on the morphology was observed for annealing at 850 °C or lower temperature (not shown). While both the $(UNCD)_0$ and $(Fe/UNCD)_{900}$ films contain fine-grain granular structure, the latter have 5–10 nm particles (showing bright contrast) lying on the surface of UNCD films (Fig. 1(b)). These small nanoparticles could be the Fe or Fe_3C nanoparticles formed by the reaction of Fe with diamond when annealed at high temperature[14–16] as discussed later. The occurrence of the new phase like Fe_3C is also evident from the GIXRD pattern of the $(Fe/UNCD)_{900}$ film, shown in Fig. 2. This shows three strongest peaks at 43.99°, 55.99°, and 75.48°, which correspond to the diamond (111), Fe_3C (212), and Fe_3C (322) phases, respectively.[20,21] It should be noted that although the granular structure of the as-deposited UNCD films is markedly different from those of the MCD films,[15] the nature of Fe-to-diamond interaction seems to be similar.

EFE properties of $(UNCD)_0$ and $(Fe/UNCD)_{900}$ films are shown in Figure 3 with the inset indicating the corresponding F-N plots. From the current density vs. electric field (J-E) curves, it is evident that the EFE properties of $(UNCD)_0$ films are significantly enhanced by the Fe-coating/annealing processes (Fig. 3(ii) for $(UNCD)_0$ and Fig. 3(iv) for $(Fe/UNCD)_{900}$). The turn-on field (E_0) decreased from 4.95 V/μm for $(UNCD)_0$ films to 1.98 V/μm for $(Fe/UNCD)_{900}$ films. A current density (J_e) of 705 $\mu A/cm^2$ at an electric field of 7.5 V/μm is measured for $(Fe/UNCD)_{900}$ films, whereas the J_e value for $(UNCD)_0$ films is only 9 $\mu A/cm^2$ at 7.5 V/μm. The EFE properties of $(Fe/UNCD)_{900}$ films is comparable to those of as-prepared carbon nanotubes (CNTs).[21–23] To facilitate the comparison, the EFE properties of the as-grown and Fe-

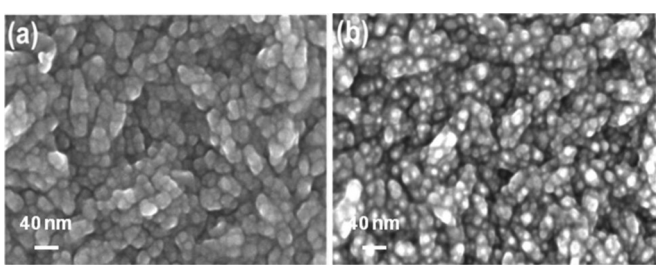

FIG. 1. FESEM image of (a) $(UNCD)_0$ and (b) $(Fe/UNCD)_{900}$ UNCD films. Presence of Fe nanoparticles is clearly seen as white contrast on the surface of UNCD films in (b).

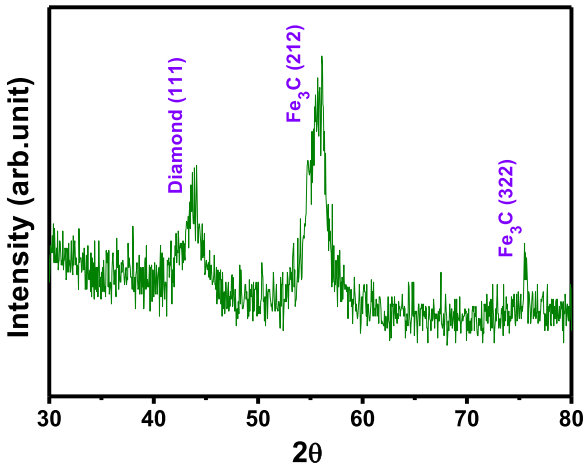

FIG. 2. GIXRD pattern of $(Fe/UNCD)_{900}$ films showing the presence of Fe_3C phase on the surface.

coated/annealed MCD films[15] are also plotted in Fig. 3. This figure indicates that the EFE properties of the $(Fe/UNCD)_{900}$ films are better than Fe-coated/annealed MCD films that may be due to the unique microstructure of UNCD films. The EFE properties of the samples are summarized in Table I.

The changes in bonding structures of the UNCD films due to the Fe-coating/annealing processes were revealed by Raman and XPS measurements. The Raman spectra of $(UNCD)_0$ and $(Fe/UNCD)_{900}$ films are shown in Figure 4. Contrary to the phenomenon that the Raman spectra of MCD films were predominated with sharp D-band at 1332 cm^{-1}, the characteristic Γ_{2g} Raman resonance of diamond crystals,[14–16] the Raman spectra of $(UNCD)_0$ films contain broad peak positions at 1143, 1333, 1364, 1481, and 1549 cm^{-1}, which are marked as ν_1, D*, D, ν_3, and G, respectively (curve I, Fig. 4). The broadness of the Raman resonance peaks is due to the smallness in grain size of the films.[24] The D-band (1333 cm^{-1}) resonance peak corresponding to Γ_{2g} Raman resonance of diamond crystals is very small. The υ_1 and υ_2 bands represent the trans-polyacetylene phase located at grain boundaries, whereas the D* and G are the characteristics of graphitic phases.[25] The Fe-coating/annealing processes insignificantly alter the Raman spectra of the UNCD films (curve II, Fig. 4).

TABLE I. The EFE properties of the as-deposited and Fe-coated/annealed MCD/ UNCD films.

Samples	Turn-on field (E_0 in V/μm)	Current density at 7.5 V/μm (J_e in $\mu A/cm^2$)
As prepared UNCD film	4.95	9
$(Fe/UNCD)_{900}$	1.98	705
As prepared MCD film[a]	5.12	<1.0
$(Fe/MCD)_{900}$[a]	3.42	170

[a]The EFE parameters of the as-prepared MCD films and $(Fe/MCD)_{900}$ were deduced from Ref. 15.

Figures 5(a) and 5(b) show the XPS C1s spectra of $(UNCD)_0$ and $(Fe/UNCD)_{900}$ films, respectively. XPS measurements were done without Ar^+ ion sputtering to avoid reconfiguration of the surface bonding structures. The background was subtracted using Shirley's method.[26] The data were fitted with Lorentzian peaks with binding energies at 284.4, 285, and 286.1 eV corresponding to sp^2, sp^3, and C-O(C-O-C) bonding of the C1s spectra,[6] respectively. Table II depicts the relative intensities of each element from the C1s spectra. The XPS C1s spectra shows the sp^2 phase fraction was only 18.5% in $(UNCD)_0$ films and significantly increased to 71.6% after the Fe-coating/annealing process in $(Fe/UNCD)_{900}$ films. The sp^3 phase fraction is 68.6% in $(UNCD)_0$ films and decreased to 23.6% in $(Fe/UNCD)_{900}$ films. A little amount of CO/C–O–C peaks were seen in as-deposited and post-annealed Fe/UNCD films at binding energy of 286.1 eV, which disappeared as soon as the surface was Ar^+ ion sputtered for 1 min in XPS chamber. The CO/C–O–C peaks may be due to the presence of oxide layers on the Fe-coated UNCD films.

Fe2p XPS spectra of $(Fe/UNCD)_{900}$ films are shown in Figure 6. Fe $2p_{3/2}$ and $2p_{1/2}$ spectra are shown by strip

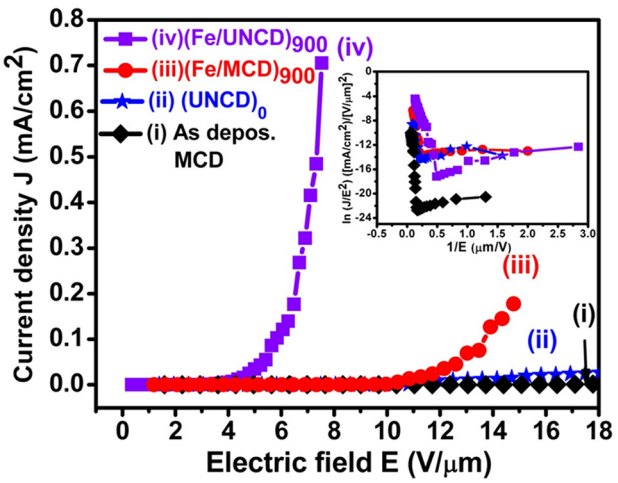

FIG. 3. EFE properties of (ii) $(UNCD)_0$ and (iv) $(Fe/UNCD)_{900}$ films. Inset shows the F-N plots derived from the corresponding J-E curves. The EFE properties of as-prepared and 900 °C Fe-coated/annealed MCD, $(Fe/UNCD)_{900}$ films, were included as curves (i) and (ii), respectively, to facilitate the comparison.

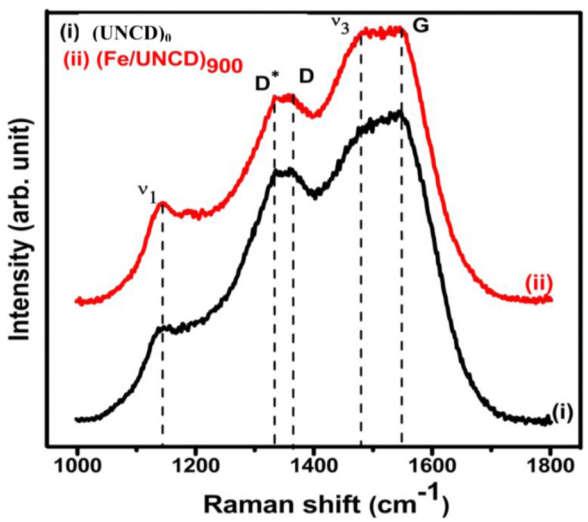

FIG. 4. Raman spectra of (i) $(UNCD)_0$ and (ii) $(Fe/UNCD)_{900}$ films.

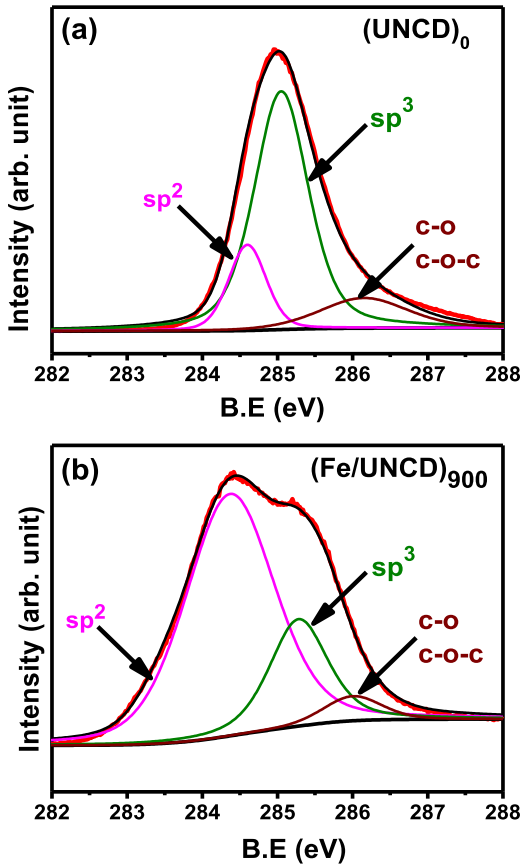

FIG. 5. The XPS C1s spectra of (a) $(UNCD)_0$ and (b) $(Fe/UNCD)_{900}$ films. The enhanced sp^2 phase is clearly seen from $(Fe/UNCD)_{900}$ spectra.

marked area. The data were fitted with Lorentzian peaks with binding energies at 707.1, 708.2, and 711.1 eV, corresponding to the Fe^0, Fe_3C, and Fe_2O_3 phases of the Fe $2p_{3/2}$ peak, respectively.[27,28] The relative peak intensities obtained from the Fe $2p_{3/2}$ spectra are also summarized in Table II. As shown in Fig. 6 and Table II, the peak intensities of Fe^0 and Fe_3C phases are 49.6% and 39.2% for $(Fe/UNCD)_{900}$ films. The presence of Fe_2O_3 phase (11.2%) is in accord with the occurrence of CO/C–O–C peaks in XPS C1s spectra. One possible reason for the presence of Fe_2O_3 phase on the Fe coated UNCD films is the oxidation of Fe-particles, which occurred instantaneously when the Fe-coated films were taken from the sputtering chamber to the annealing setup. It should be noted that the concentration of sp^2, Fe (Fe_3C) phases are more in $(Fe/UNCD)_{900}$ films than $(Fe/MCD)_{900}$

TABLE II. The C1s and Fe 2p XPS peaks of $(UNCD)_0$ and $(Fe/UNCD)_{900}$ films.

		Peak intensity (%)	
Peak position (eV)	Chemical bonding	$(UNCD)_0$	$(Fe/UNCD)_{900}$
284.4	sp^2	18.5	71.6
285.0	sp^3	68.6	23.6
286.1	C-O (or C-O-C)	12.9	4.8
707.1	Fe^0	…	49.6
708.2	Fe_3C	…	39.2
711.1	Fe_2O_3	…	11.2

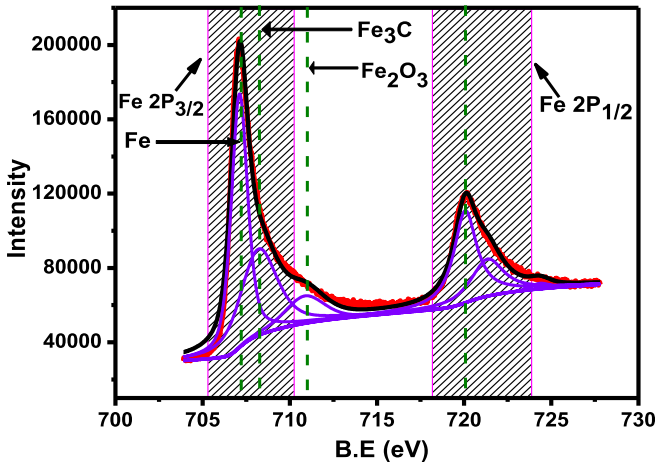

FIG. 6. Fe2p XPS spectra of $(Fe/UNCD)_{900}$ film.

films[15] that is presumed to be the factors responsible for better EFE properties for $(Fe/UNCD)_{900}$ films than $(Fe/MCD)_{900}$ films.[14–16] How the increased sp^2 and Fe (Fe_3C) phase contents significantly affect the EFE properties for the $(Fe/UNCD)_{900}$ films than $(Fe/MCD)_{900}$ films are discussed shortly.

B. Transmission electron microscopy

It should be noted that the XPS spectra represent mostly the surface characteristics of the films that is not necessary the same as the phases contained in the films. The understanding of the microstructural evolution induced by the Fe-coating/annealing processes is actually more important. For such purpose, the microstructure of the $(Fe/UNCD)_{900}$ films were examined using TEM. Figure 7(a) shows the typical bright field (BF) image for the $(Fe/UNCD)_{900}$ films acquired in STEM. Inset in Fig. 7(a) shows the selected area electron diffraction (SAED) pattern of the same region acquired in TEM mode. The diffraction spots are arranged in a smooth ring, implying that this region mainly contains randomly oriented ultra-small diamond grains.

By changing the camera length (CL) in the STEM, the electrons incoherently (but elastically) scattered by different species can be resolved, provided that the correlation between the scattering angle and the atomic number of the species inducing the incoherently scattering process was known. For the $(Fe/UNCD)_{900}$ films shown in Fig. 7(a), only iron and carbon (diamond, graphite, or amorphous carbon) species were involved. The contribution of the two species can be clearly resolved by changing the CL in acquiring the HAADF signals. Figure 7(b) illustrates a typical composed-HAADF image, which is superposition of three HAADF images acquired using different CL-values, $CL_1 = 400$ mm (yellow color), $CL_2 = 127.3$ mm (blue color), and $CL_3 = 93$ mm (red color). The energy-dispersive X-ray spectroscopy (EDX) patterns (in STEM mode) corresponding to the yellow, pink, and red regions designated as 1 to 6 in Fig. 7(b) are plotted as profiles 1 to 6 in Fig. 8, respectively. These EDX patterns clearly indicate that the profiles 1 and 2 corresponding to locations 1 and 2 contain mostly the carbon, revealing that the yellow-colored regions are diamond

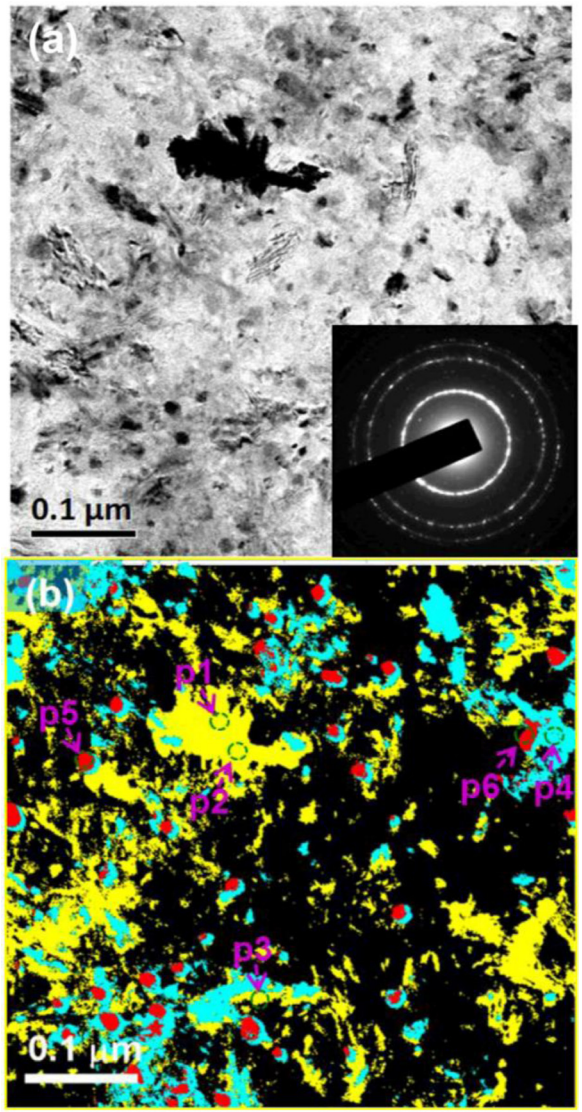

FIG. 7. The (a) STEM BF and (b) HAADF images corresponding to BF image for $(Fe/UNCD)_{900}$ film.

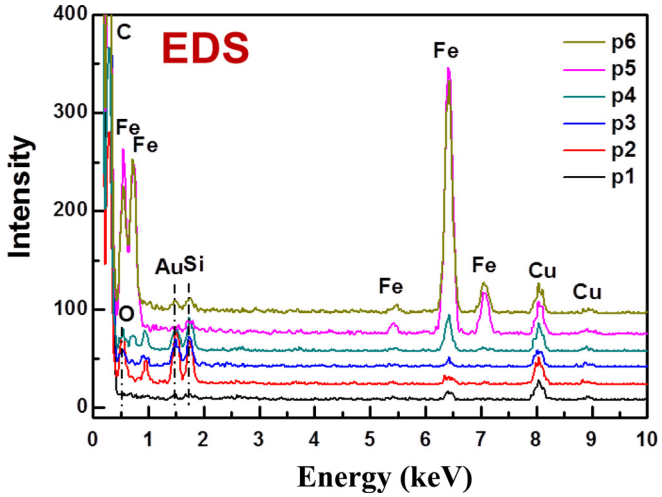

FIG. 8. The EDX (STEM) profiles for $(Fe/UNCD)_{900}$ film. The spectra 1 to 6 correspond to the locations 1 to 6 designated in Fig. 7(b).

(or graphite), whereas the EDX profiles 5 and 6 corresponding to locations 5 and 6 contains large Fe-signals, indicating that the red-colored region, which corresponds to smallest CL-value ($CL_3 = 93$ mm), is mainly Fe-clusters. The EDX profiles 3 and 4 corresponding to locations 3 and 4 contains both Fe and C signals, implying this blue-colored region might be the compound of Fe and C, most probably, the Fe_3C-clusters. The small Cu, Au, and Si signals are presumably the contaminations from the underlying substrates and the Cu-mesh induced in the ion-milling process.

The more important microstructural information, such as the geometry and distribution of these phases, is needed to understand the authentic factor that enhanced the EFE behavior for the Fe-coated/annealed UNCD films. For this purpose, the HAADF technique for identifying the distribution of species in $(Fe/UNCD)_{900}$ films is investigated by utilizing the 3D-tomography in TEM. The 3D-tomography is a series of HAADF images taken with the samples tilted step wisely (2° per step) and then replayed sequentially using DIGITAL-MICROGRAPH (JEOL)[19] software. Figure 9(a) shows the stereographic projection of the 3D tomography for the $(Fe/UNCD)_{900}$ film, whereas Fig. 9(b) shows the X-Y projection of this image. These micrographs illustrate more clearly that the Fe (red color), Fe_3C (white color), and nanocarbon clusters (nanodiamond or nanographite, yellow color) are of spherical geometry and are located on the surface of the UNCD films. The Fe, Fe_3C, and nanocarbon clusters, about tens of nanometers in size, are mixed together, implying that, while some of the Fe-clusters interacted with diamond, forming Fe_3C, some of them remained intact. These figures show that the nano-graphitic phase actually formed in adjacent to the Fe_3C (or Fe) clusters. These observations support the arguments that the graphitic phase was induced by Fe-to-diamond interaction, forming a continuous network. The presence of the interconnected conducting network facilitated the electron transport and enhanced the EFE properties.

It should be noted that although the Fe-coating also formed nano-sized clusters prior the interaction with the diamond in MCD films, the distribution of Fe_3C and Fe clusters formed on the faceted MCD grains[15] is distinctly different from those observed in Fig. 9 on the UNCD films. For MCD films, the faceted diamond grains are large. The Fe clusters cover the whole flat surface of the grains and interact with the diamond simultaneously, resulting in a layer of Fe-clusters on top of the Fe_3C layer.[15] In contrast, in the UNCD films, the equi-axed grains are extremely small, about 5 nm in size.[29] The Fe-clusters, about the same size as UNCD grains, were formed on top of each grain (cf. Fig. 1(b)). The size of Fe-clusters formed on UNCD films is markedly smaller as compared with that formed on MCD films.[15] The diffusion length for carbon is markedly smaller that more efficiently induced the formation of nano-sized graphite clusters, surrounding each Fe-clusters. The Fe, Fe_3C, and nano-graphite clusters formed in $(Fe/UNCD)_{900}$ films that were mixed up rather than forming a Fe-layer on top of Fe_3C layer as in $(Fe/MCD)_{900}$ films. The nano-graphite clusters in $(Fe/UNCD)_{900}$ films are not only smaller in size but also more densely populated. The number density of nano-graphitic clusters is about the same order of magnitude as the number of nano-sized diamond grains in UNCD films. The finer and

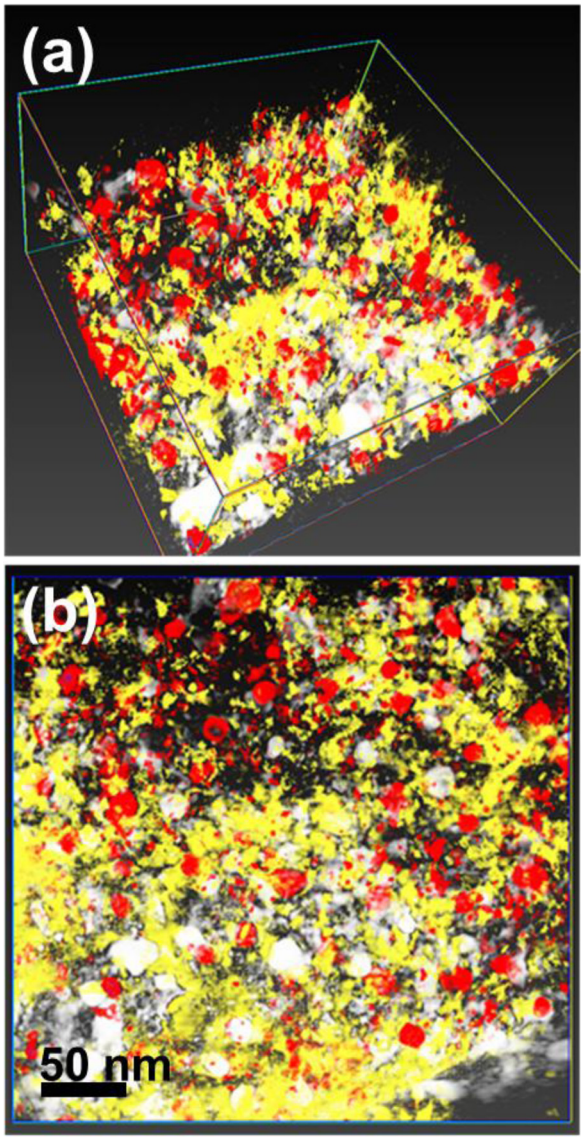

FIG. 9. (a) The stereographic projection and (b) X-Y projection of the TEM 3D-tomography of $(Fe/UNCD)_{900}$ film.

more densely populated nanographite clusters formed in UNCD films is the authentic factor that resulted in superior EFE properties for the UNCD films comparing to those for MCD films.

C. Scanning tunneling spectroscopy

To reveal how the change in microstructure and concentrations of sp^2, sp^3, Fe (or Fe_3C) phases significantly affect the EFE properties in a microscopic scale, the local electronic properties of these films were investigated by STS. STS measurements of $(UNCD)_0$ and $(Fe/UNCD)_{900}$ films are illustrated to reveal the modification in surface electronic properties due to the Fe-coating/annealing processes. Figure 10(a) shows the image of an as-deposited UNCD film. It seems that the small diamond grains in as-deposited UNCD films merged with each other and forms a bunch, marked as point "1" in Fig. 10(a). Bright and dark contrasts are seen in the corresponding CITS image taken at the sample bias of −1.8 V (Fig. 10(b)). Bright contrast in the CITS image

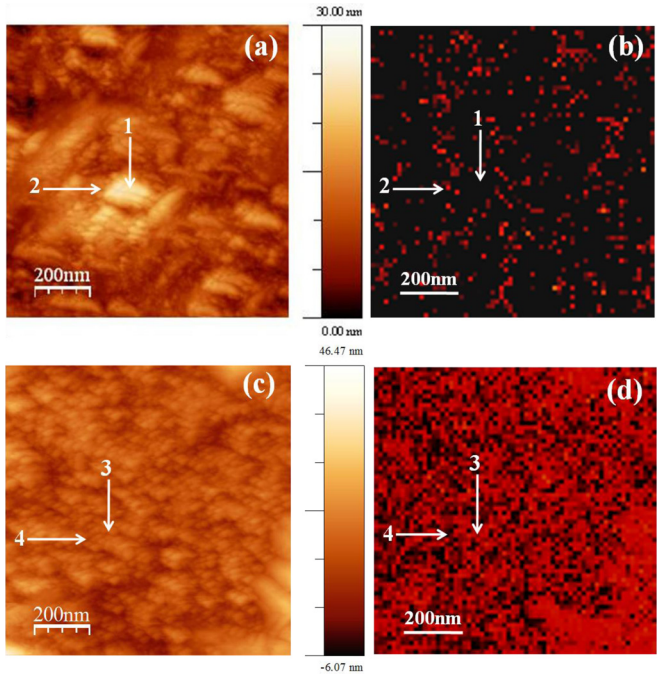

FIG. 10. (a) UHV STM image of $(UNCD)_0$ films with the corresponding CITS image in (b). (c) $(Fe/UNCD)_{900}$ film with corresponding CITS image in (d). Enhanced emission sites of $(Fe/UNCD)_{900}$ film is clearly seen in CITS image (d) than $(UNCD)_0$ in (b).

shows better electron emission.[6] The emission sites are seen around the boundaries of the bunch of diamond grains as seen from the CITS image shown in Fig. 10(b). The $(UNCD)_0$ films show few bright spots indicating less emission sites on the surface.[6] In contrast, the STM surface morphology of $(Fe/UNCD)_{900}$ film with its corresponding CITS image, are shown in Figs. 10(c) and 10(d), respectively. Small nano-particles, which are presumed to be the Fe (or Fe_3C) clusters, covering the whole UNCD surface, are seen from the STM image in Fig. 10(c). The CITS image, taken at the same sample bias (Fig. 10(d)), shows significant increase in emission sites than $(UNCD)_0$ films shown in Fig. 10(b). A typical bunch of diamond grain with grain boundary is marked as "3" and "4," respectively, in Figs. 10(c) and 10(d). Interestingly, the emission sites are seen throughout the diamond grains in $(Fe/UNCD)_{900}$ film rather than only from the boundaries, as in case of $(UNCD)_0$ films, shown in Fig. 10(b).

To reveal the actual emission sites in $(Fe/UNCD)_{900}$ films, the CITS images from the region 3 in Fig. 10(c) were more detailed examined. The HRSTM image and its corresponding CITS image are shown in Figs. 11(a) and 11(b), respectively. Nanoparticles of various sizes (~5-10 nm) are seen in $(Fe/UNCD)_{900}$ film surface as shown in Fig. 11(a). They could be the Fe (or Fe_3C) nanoparticles as observed during TEM studies. Notably, the size of Fe (or Fe_3C) nanoparticles is similar with those for the nano-sized diamond grains in UNCD films that are in accord with the SEM and TEM observations. Interestingly, significant increase in emission sites are observed in $(Fe/UNCD)_{900}$ films as more bright spots are seen around the Fe (or Fe_3C) nanoparticles shown in Fig. 11(b). Moreover, not only the emission site

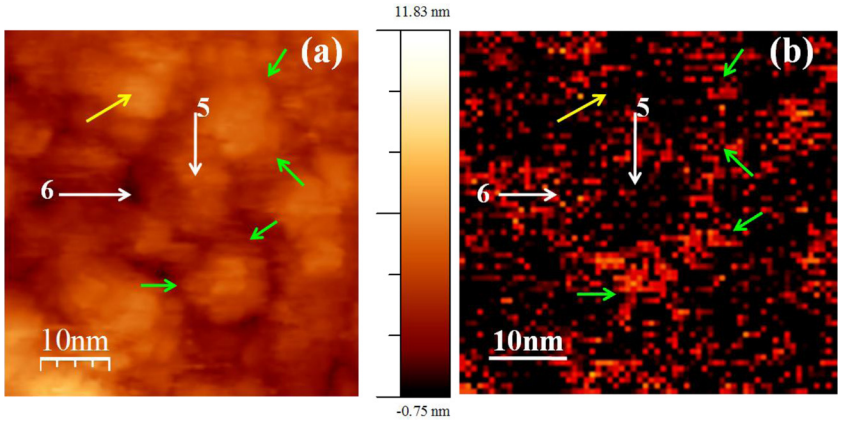

FIG. 11. (a) High resolution STM image and (b) the corresponding CITS image for $(Fe/UNCD)_{900}$ film.

density increases but also the width of the bright spots increases as shown by green arrow marks in Fig. 11(b). This fact is also consistent with the TEM results, which show the formation of nano-graphitic phases along the boundaries of Fe (Fe_3C) nanoparticles. These nanographitic phase at boundaries help in easy transport of electrons around the Fe (or Fe_3C) nanoparticles and thus makes interconnected path throughout the sample surfaces due to their high densities as seen in CITS image in Fig. 10(d).

To get more insight into the local electronic properties of as-deposited and Fe coated/annealed films, the local current-voltage (I-V) curves are taken in STS mode from various sample positions and are shown in Fig. 12(a). Only the negative portion of the I-V curves are shown in Fig. 12(a), since the negatively biased current represents the tunneling of electrons from the diamond surface to the tungsten tip and is proportional to the density of occupied states of diamond. Two reproducible I-V spectra were recorded during the scanning of the $(Fe/UNCD)_{900}$ film. The reproducible I-V spectra (10 each) are shown by open symbols and the average of these curves are plotted as solid symbols. The I-V spectra taken from nanoparticles (marked as "5" in Fig. 11(a)) show a current value of 30 nA at −1.6 V as shown in curves "i" in Fig. 12(a). These nano-sized particles could be the Fe_3C particles, as seen in TEM observation. Conductivity at the boundaries of the Fe (Fe_3C) nanoparticles (marked as "6" in Fig. 11(a)) show ohmic behavior (curves "ii" in Fig. 12(a)). These boundaries could be the nanographitic phase surrounding the Fe (Fe_3C) nanoparticles, also evidenced from TEM study. Significant conductivity has been measured (30 nA at −0.6 V) from these positions. It is to be noted here that for diamond grains in $(UNCD)_0$ films (e.g., "1" in Fig. 10(a)), it requires higher bias of −2.9 V to get a value of 30 nA tunneling current (not shown). The enhanced tunneling current from the boundaries of Fe, Fe_3C nanoparticles in Fe coated/annealed UNCD films also explains the superior EFE properties of $(Fe/UNCD)_{900}$ than the $(UNCD)_0$ films in a microscopic scale.

Figure 12(b) shows the normalized conductance $\frac{dI/dV}{I/V}$ versus sample bias (V) curves, which are calculated from the I-V characteristic curves and provides information about the distribution of the surface DOS[30,31] of the film. The normalized conductance spectra corresponding to the curves "i" and "ii" in Fig. 12(a) are shown in Fig. 12(b). Band gap calculations on the nanoparticle (marked as "5" in Fig. 11(a)) show very small band gap (0.16 eV, curve "i," Fig. 12(b)). The normalized conductance curve "ii" in Fig. 12(b), shows nearly zero band gap (metallic type) for the boundaries, which are marked as point "6" in the HRSTM image (cf. Fig. 12(a)). These are, presumably, the nanographitic phases surrounding the Fe or Fe_3C nanoparticles which are also evidenced from TEM study. Restated, the nanographitic phase present at the boundary of these Fe (or Fe_3C) nanoparticles

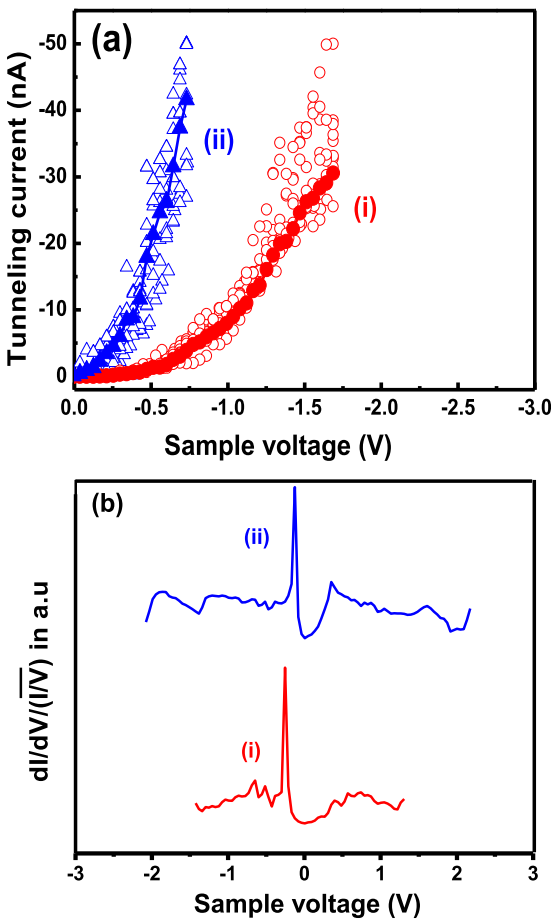

FIG. 12. (a) The I-V characteristic curves (thick curve represents the average over the 10 I-V curves at each mentioned point) and (b) normalized differential conductance (dI/dV)/(I/V) curves at various locations: on (i) the nanoparticles marked as "5" in Fig. 11(a) and (ii) boundaries of nanoparticles, marked as "6" in Fig. 11(a) of $(Fe/UNCD)_{900}$ films.

seems to be the main conducting channel for the electrons in $(Fe/UNCD)_{900}$ films.

In ultrananocrystalline diamond films, the electrons are transported along the grain boundaries of the nano-sized diamond grains and are emitted from these sites.[32,33] However, in as-deposited UNCD films, most of the grain boundaries contain the trans-polyacetylene or amorphous carbon phase, which are not very conductive for efficient transporting the electrons. Interestingly, in $(Fe/UNCD)_{900}$ films, nanographitic phases are formed around the Fe (or Fe_3C) nanoparticles, which are formed by the reaction of Fe with diamond when the Fe coated UNCD films are annealed at 900 °C. The formation mechanism of nanographitic phase on the Fe coated UNCD film is similar to that in Fe-coated MCD films.[15] Presumable, the Fe-clusters catalytically dissociated the diamond at temperature of 900 °C, transported the carbon species through the Fe-clusters, and reprecipitated them out at the other side of the Fe-clusters, resulting in nanographite on the surface of these Fe clusters. The Fe_3C nano-clusters were resulted, when the Fe nanoparticles containing some dissolved carbons are quickly cooled below the re-precipitation temperature.

More importantly, the concentration of the Fe (or Fe_3C) nanoparticles is more when the Fe coated UNCD films are annealed at 900 °C in H_2 atmosphere, as compared with those in Fe-coated MCD films.[15] The presence of nanographitic phase around the Fe (or Fe_3C) nanoparticles in $(Fe/UNCD)_{900}$ samples is presumed to serve as an electron transport medium as well as electron emission sites. Furthermore, the $(Fe/UNCD)_{900}$ films show markedly superior EFE properties, i.e., smaller turn-on field (E_0) and larger EFE current density (Je), comparing to those for $(Fe/MCD)_{900}$ films.[15] The TEM and STM studies indicate that markedly larger emission site density for the $(Fe/UNCD)_{900}$ films is resulted from the higher number density of nano-graphite (Fe and Fe_3C) clusters formed on the $(Fe/UNCD)_{900}$ films. The authentic factor resulting in more favorable nano-graphite (Fe and Fe_3C) clusters distribution is apparently owing to the unique nano-sized granular structure, viz. ultra-small grain size and uniform grain size distribution, comparing to the faceted grain microstructure for MCD films, as discussed previously.

IV. CONCLUSIONS

A thin layer of Fe-coating and post-annealing at high temperature of 900 °C is seen to modify the surface characteristics and significantly enhance the EFE properties of UNCD films. The increased number densities of emission sites in $(Fe/UNCD)_{900}$ films than the as-deposited one are clearly observed from the CITS images. Microstructural analysis indicates that the mechanism behind the enhanced EFE properties is the formation of nanographitic phase at the boundaries of the Fe (or Fe_3C) nanoparticles, which are formed via the reaction of Fe clusters with UNCD films during the annealing process. These nanographitic phases are presumed to serve as an electron transport medium as well as electron emission sites. Furthermore, the improved emission properties arising due to the nanographitic phase in $(Fe/UNCD)_{900}$ films are also directly confirmed from the high resolution CITS images. XPS measurements reveal the concentration of Fe (or Fe_3C) phases and sp^2 phase fractions are more in 900 °C Fe-coated/post-annealed UNCD films that facilitate the EFE properties. The Fe-coating/annealing processes enhanced the EFE properties of UNCD films more than that on the MCD films. The authentic factor, resulting in such a phenomenon, is attributed to the unique granular structure of the UNCD films. The nano-sized and uniformly distributed grains of UNCD films resulted in markedly smaller and densely populated Fe-clusters, which, in turn, induced more finer and higher populated nano-graphite clusters. The Fe-coated/post-annealed UNCD films with better EFE properties open up a new path way for the development of next generation high-definition flat panel displays.

ACKNOWLEDGMENTS

The authors would like to thank Mr. Nandagopala Krishna for XPS, Mr. P. Shyamala Rao for FESEM, and Sujoy Chakravarty, UGC-DAE CSIR, Kalpakkam node for GIXRD experiments. National Science Council, Republic of China is greatly acknowledged for the support of this research through the Project No. NSC 99-2119-M-032- 003-MY2.

[1]J. E. Field, *The Properties of Diamonds* (Academic, London, 1979).
[2]H. Liu and D. S. Dandy, Diamond Relat. Mater. **4**, 1173 (1995).
[3]J. C. Angus, H. A. Will, and W. S. Stanko, J. Appl. Phys. **39**, 2915 (1968).
[4]B. V. Spitsyn, L. L. Bouilov, and B. V. Derjaguin, J. Cryst. Growth **52**, 219 (1981).
[5]F. J. Himpsel, J. A. Knapp, J. A. Van Vechten, and D. E. Eastman, Phys. Rev. B **20**, 624 (1979).
[6]K. Panda, B. Sundaravel, B. K. Panigrahi, P. Magudapathy, D. N. Krishna, K. G. M. Nair, H.-C. Chen, and I.-N. Lin, J. Appl. Phys. **110**, 044304 (2011).
[7]O. Auciello and A. V. Sumant, Diamond Relat. Mater. **19**, 699 (2010).
[8]O. A. Williams, Semicond. Sci. Technol. **21**, R49 (2006).
[9]S. Fan, M. G. Chapline, N. R. Franklin, T. W. Tombler, A. M. Cassell, and H. Dai, Science **283**, 512 (1999).
[10]S. Pandey, P. Rai, S. Patole, F. Gunes, G. D. Kwon, J. B. Yoo, P. Nikolaev, and S. Arepalli, Appl. Phys. Lett. **100**, 043104 (2012).
[11]M. Qian, T. Feng, H. Ding, L. Lin, H. Li, Y. Chen, and Z. Sun, Nanotechnology **20**, 425702 (2009).
[12]A. Lamouri, Y. Wang, G. T. Mearini, I. L. Krainsky, J. A. Dayton, and W. Mueller, J. Vac. Sci. Technol. B **14**, 2046 (1996).
[13]I. N. Lin, Y. H. Chen, and H. F. Cheng, Diamond Relat. Mater. **9**, 1574 (2000).
[14]P. C. Huang, W. C. Shih, H. C. Chen, and I. N. Lin, Jpn. J. Appl. Phys., Part 1 **50**, 08KE04 (2011).
[15]K. Panda, B. Sundaravel, B. K. Panigrahi, P. C. Huang, W. C. Shih, H. C. Chen, and I. N. Lin, J. Appl. Phys. **111**, 124309 (2012).
[16]P. C. Huang, W. C. Shih, H. C. Chen, and I. N. Lin, J. Appl. Phys. **109**, 084309 (2011).
[17]W. Kern, J. Electrochem. Soc. **137**, 1887 (1990).
[18]R. H. Fowler and L. Nordheim, Proc. R. Soc. London, Ser. A **119**, 173 (1928).
[19]See http://www.jeolusa.com/RESOURCES/ElectronOptics/DocumentsDownloads/tabid/320/Default.aspx?EntryId=800 for the information of digital-micrograph (JEOL) software.
[20]E. J. Fasika and G. A. Jeffrey, Acta Crystallogr. **19**, 463 (1965).
[21]J. Thewlis and A. R. Davey, Phil. Mag. Lett. **1**, 409 (1956).
[22]H. F. Cheng, Y. M. Tsau, T. Y. Chang, T. S. Lai, T. F. Kuo, and I.-N. Lin, Diamond Relat. Mater. **12**, 486 (2003).
[23]B. B. Wanga, Q. J. Cheng, X. Chen, and K. Ostrikovb, J. Alloys Compd. **509**, 9329 (2011).

[24]D. Zhou, D. M. Gruen, L. C. Qin, T. G. McCauley, and A. R. Krauss, J. Appl. Phys. **84**, 1981 (1998).
[25]A. C. Ferrari and J. Robertson, Phys. Rev. B **61**, 14095 (2000).
[26]Y. F. Chen, Surf. Sci. **380**, 199 (1997).
[27]Y. Kai-yu, X. Wei, Z. Yu, Z. Wei-tao, and W. Xin, Chem. Res. Chin. Univ. **26**(3), 348 (2010).
[28]T. Fujii, F. M. F. de Groot, and G. A. Sawatzky, Phys. Rev. B **59**, 3195 (1999).
[29]I. N. Lin, H. C. Chen, C. S. Wang, Y. R. Lee, and C. Y. Lee, CrystEngComm **13**, 6082 (2011).
[30]R. M. Feenstra, Surf. Sci. **965**, 965 (1994).
[31]R. M. Feenstra and P. Martenssion, Phys. Rev. Lett. **61**, 447 (1988).
[32]M. W. Geis, N. N. Efremow, J. D. Woodhouse, M. D. Mcaleese, M. Marchywka, D. G. Socker, and J. F. Hochedez, IEEE Electron Device Lett. **12**, 456 (1991).
[33]R. Krauss, O. Auciello, M. Q. Ding, D. M. Gruen, Y. Huang, V. V. Zhirnov, E. I. Givargizov, A. Breskin, R. Chechen, E. Shefer, V. Konov, S. Pimenov, A. Karabutov, A. Rakhimov, and L. N. Suetin, J. Appl. Phys. **89**, 2958 (2001).